Crystal Structure of Human Phosphodiesterase 3B: Atomic Basis for Substrate and Inhibitor Specificity†

Giovanna Scapin,*,‡ Sangita B. Patel,‡ Christine Chung,§ Jeffrey P. Varnerin,§ Scott D. Edmondson,‡ Anthony Mastracchio,‡ Emma R. Parmee,‡ Suresh B. Singh,‡ Joseph W. Becker,‡ Lex H. T. Van der Ploeg,|| and Michael R. Tota§

Departments of Medicinal Chemistry and Metabolic Disorders, Merck & Co., Rahway, New Jersey 07065, and MRL San Diego Neuroscience Center, San Diego, California 92121

Received January 16, 2004; Revised Manuscript Received March 17, 2004

ABSTRACT: Phosphodiesterases (PDEs) are enzymes that modulate cyclic nucleotide signaling and as such are clinical targets for a range of disorders including congestive heart failure, erectile dysfunction, and inflammation. The PDE3 family comprises two highly homologous subtypes expressed in different tissues, and inhibitors of this family have been shown to increase lipolysis in adipocytes. A specific PDE3B (the lipocyte-localized subtype) inhibitor would be a very useful tool to evaluate the effects of PDE3 inhibition on lipolysis and metabolic rate and might become a novel tool for treatment of obesity. We report here the three-dimensional structures of the catalytic domain of human PDE3B in complex with a generic PDE inhibitor and a novel PDE3 selective inhibitor. These structures explain the dual cAMP/cGMP binding capabilities of PDE3, provide the molecular basis for inhibitor specificity, and can supply a valid platform for the design of improved compounds.

PDEs[1] are a large family of enzymes that catalyze hydrolysis of the 3′−5′ phosphodiester bond of cyclic nucleotides (cAMP and cGMP), therefore providing a major pathway for modulating cyclic nucleotide signaling (*1*). Changes in the intracellular concentration of cyclic nucleotides mediate the actions of numerous hormones and neurotransmitter signals important for cell growth, differentiation, survival, and inflammation (*2*). At least 11 families of PDEs with varying selectivities for cAMP or cGMP have been identified in mammalian tissues. Within these families, multiple isoforms are expressed either as products of different genes or as products of the same gene through alternative splicing (*2*). The PDE3 subfamily consists of two closely related subtypes: PDE3A and PDE3B. While PDE3A is mostly expressed in cardiac tissue, platelets, and vascular smooth muscle cells, PDE3B is prevalently expressed in hepatocytes and adipose tissue (*3*). While several PDE families are highly selective for either cAMP or cGMP, PDE3 accommodates both. Because the two nucleotides compete for the same catalytic site, the PDE3 family has been given the name of cGMP-inhibited PDE. cGMP has a K_i of ∼0.2 μM, and this competition probably plays an important role in controlling the intracellular levels of cAMP and cGMP (*2*). PDE3B is a key agent in the stimulatory action of cAMP on pancreatic β-cell exocytosis and release of insulin (*4*). cAMP potentiates glucose-stimulated insulin release and mediates the stimulatory effects of hormones such as glucagon-like peptide 1 on pancreatic β-cells. PDE3 inhibitors have been shown to increase lipolysis in adipocytes. A specific PDE3B inhibitor would be a very useful tool to evaluate the effects of PDE3B inhibition on lipolysis and metabolic rate increase, and such an inhibitor might be a novel tool for the treatment of obesity (*5*, *6*). Although PDE3B is a membrane-associated protein, the catalytic domain can be independently expressed as a soluble enzyme that retains catalytic activity (*7*−*10*). Given the fact that different PDEs can be targeted for different therapeutic reasons, it is necessary to understand the reasons for the specificity of these enzymes and to address the issue of selective inhibitors. The only available PDE family crystal structures to date are those of PDE4B2B (*11*), PDE4D (*12*, *13*), and PDE5A (*14*). To facilitate the development of compounds specifically targeting the 3B isoform, we undertook structural studies of the PDE3B catalytic domain. We report here the three-dimensional structures of PDE3B in complex with a generic PDE inhibitor and a novel subtype selective inhibitor. These structures provide insights into the enzyme's dual cAMP/cGMP affinity and will allow for the design of more potent and selective PDE3B inhibitors.

MATERIALS AND METHODS

Protein Expression and Purification. The catalytic domain of PDE3B has been expressed and purified as previously reported (*9*). Dynamic light scattering analysis was performed using a Protein Solutions LTD (High Wycombe, U.K.)

† The facilities at IMCA-CAT are supported by the companies of the Industrial Macromolecular Crystallography Association through a contract with the Illinois Institute of Technology (IIT), executed through IIT's Center for Synchrotron Radiation Research and Instrumentation. Use of the Advanced Photon Source was supported by the U.S. Department of Energy, Basic Energy Sciences, Office of Science, under Contract No. W-31-109-Eng-38.

* To whom correspondence should be addressed. Tel: 732-595-8429. Fax: 732-594-5042. E-mail: giovanna_scapin@merck.com.

‡ Department of Medicinal Chemistry, Merck & Co..

§ Department of Metabolic Disorders, Merck & Co..

|| MRL San Diego Neuroscience Center.

[1] Abbreviations: PDE, phosphodiesterase; cAMP, cyclic adenosine monophosphate; cGMP, cyclic guanosine monophosphate; RMSD, root mean square deviation.

10.1021/bi049868i CCC: $27.50
Published on Web 04/27/2004

Table 1: Statistics for the Refined Structures Described in the Text[a]

ligand	IBMX	MERCK1
space group	*C*2	*C*2
unit cell parameters		
a (Å)	275.1	146.8
b (Å)	147.1	121.5
c (Å)	253.5	126.3
β (°)	109.8	100.6
resolution range (Å)	30.0−2.9	30.0−2.4
no. molecules/AU	12	4
no. reflection used in refinement	192 993 (16 290)	81 363 (8105)
no. reflection used for R_{free}	10 121 (889)	5354 (433)
R_{free}/R factor %	24.9/23.1 (40.1/38.3)	27.7/23.2 (34.1/31.8)
RMSD bond length/angle (Å/°)	0.0091/1.18	0.012/1.37
no. protein atoms	35 760	11 717
no. solvent atoms	288	362
no. heteroatoms (ligand + ions)	216	225[b]

[a] Numbers in parentheses refer to the last shell of resolution (3.0−2.9 Å for the PDE3B:IBMX complex and 2.5−2.4 Å for the PDEB:MERCK1 complex). [b] Includes four molecules of detergent Hega-9.

Dynapro Molecular Sizing Instrument. On average, 15−25 measurements were collected for each sample at 20 °C using a laser wavelength of 8307 Å and a scattering angle of 90°. The measurements were analyzed using the standard procedure (aqueous buffer, globular protein) implemented in the Dynamics Version 4.0 software.

Crystallization, Data Collection, and Processing. Crystals of PDE3B in complex with IBMX and MERCK1 were obtained as previously reported (*15*). Data for the IBMX complex were collected on a MAR Research CCD detector at beamline 17-BM in the facilities of the IMCA-CAT at the Advanced Photon Source (Argonne National Laboratory, Argonne, IL). Data for the MERCK1 complex were collected on a ADSC Q210 CCD at beamline 17-ID (*15*). All data were processed using HKL2000 (*16*).

Structure Solution and Refinement. The structure of PDE3B in complex with MERCK1 (four molecules per AU) was solved using Molecular Replacement methods [MOLREP (*17*)] and a model of PDE3B based on PDE4B (*11*) as a search model. In the search model, only side chains of residues that were conserved in the two enzymes were retained; all of the others were changed to alanine. In addition, all loops connecting secondary structure elements were removed, even if the amino acid sequence was conserved. The final search model contained 243 residues out of the total of 420 (58% of the model). The molecular replacement solution (all four molecules) had a correlation coefficient of 0.224% and an *R* factor of 56.2% for data to 4.0 Å. The resulting phases were subjected to solvent flattening and NCS averaging using DM (*18*). The ensuing maps allowed for the tracing of part of the missing loops and for primary sequence assignment. The refinement was continued alternating manual rebuilding of the model with O (*19*) and computer-based refinement with CNX [Accelrys (*20*)]. The structure of the IBMX containing complex (12 molecules per AU) was solved by molecular replacement, using MOLREP and one monomer of the refined PDE3B:MERCK1 complex. The refinement was carried out essentially as outlined for the MERCK1 complex, utilizing strict NCS during the first stages of the refinement and then switching to restrained NCS during the last cycle. Final statistics for the refined models are reported in Table 1. The coordinates and structure factors for the two structures described here have been deposited with the Protein Data Bank for immediate release upon publication, accession codes 1SO2 (MERCK1 complex) and 1SOJ (IBMX complex), respectively.

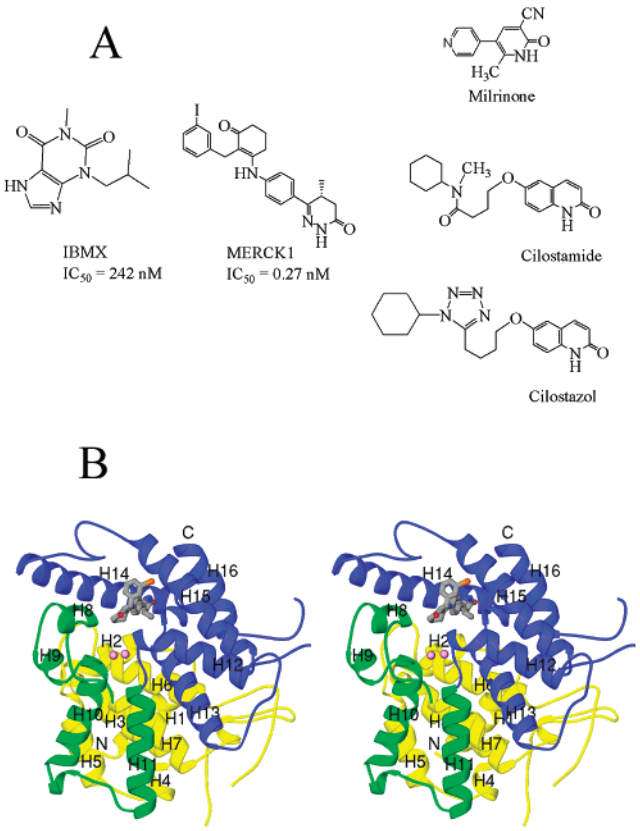

FIGURE 1: Three-dimensional structure of PDE3B. (A) Chemical structure of the inhibitors mentioned in the text. (B) Ribbon diagram of the catalytic domain of PDE3B. The 16 helices comprising the domain are numbered sequentially. The bound inhibitor is displayed as a gray ball-and-stick model. The two bound ions are displayed as purple balls. Figures 1B; 2A,B; 3A−C; 4C−E; and 5 were prepared with RIBBONS (*30*).

RESULTS

Overall Structure. The three-dimensional structure of the catalytic domain of PDE3B (residues 654−1073) in complex with MERCK1 (Figure 1A) has been solved and refined to 2.4 Å resolution. The final model contains four protein molecules, 362 water molecules, nine Mg^{2+} ions (two in each enzyme binding site and one bridging two protein molecules), and four MERCK1 molecules per asymmetric unit. The model for PDE3B in complex with IBMX (Figure 1A) contains 12 protein molecules, 12 inhibitor molecules, 288 solvent molecules, and 24 metal atoms per asymmetric unit, and it has been refined to 2.9 Å resolution. Table 1 reports the statistics for both refined complexes. Given that the structure of PDE3B is essentially identical in both complexes and that the PDE3B:MERCK1 structure has been refined to a higher resolution, this complex will be used for the general description, and differences will be pointed out when necessary. The overall structure of PDE3B is very similar to that of PDE4B (*11*), PDE4D (*12*, *13*), and PDE5A (*14*), and a similar nomenclature will be used for the description of the structure. The catalytic domain of PDE3B is compactly folded and contains 16 α-helices, which form three subdo-

mains (color-coded in Figure 1B). The amino-terminal domain (yellow in Figure 1B) is a bundle of seven helices (H1−H7) spanning residues 661−820. The first four residues of the construct used in these studies (654−658) are not visible in the electron density maps. Between helices 6 and 7, there is a 44 residue insertion (Arg755-Ser798) typical of the PDE3 subfamily (*21*). This insertion lacks any clear secondary structure organization, and residues 767−781 are not visible in the electron density maps. Helices H8−H11 form the second subdomain (green in Figure 1B). The third subdomain is composed of five α-helices (H12−H16, blue in Figure 1B) and intervening loops. Helix H15 is kinked by Pro998, as previously observed in the structures of PDE4B (*11*). Helices H15 and H16 are connected by a long stretch of poorly conserved and largely polar residues (Gly1007-Ile1057). Electron density is not available for residues 1016−1052.

The structure of PDE3B:MERCK1 complex has been solved in a monoclinic space group, with four molecules in the asymmetric unit, arranged as two independent dimers. Although the protein migrates as an apparent trimer in size exclusion chromatography (*9*), a dimeric species is evident in dynamic light scattering experiments carried out at the concentration used for crystallization (Figure 2C). The dimer (Figure 2A,B) is generated by an 180° rotation around an axis perpendicular to the "hook" formed by the two short helices H8 and H9 and intervening loop. The dimer interface is relatively small (only 1431 Å^2 are buried upon dimer formation out of the 16 370 Å^2 of solvent accessible surface of the monomer) and is formed around a hydrophobic core, which includes Leu843 and Tyr844 from both molecules. In addition, hydrogen bond interactions are formed between the side chain oxygen of Tyr844 of one molecule and the main chain oxygen of Leu843 of the other molecule and between the side chains of Asn845 and Asp846 in one molecule and Asp852 and Arg883, respectively, in the other molecule (Figure 2B). The same dimeric arrangement is present in the asymmetric unit of the PDE3B:IBMX complex. In the MERCK1 complex, four molecules of a detergent (Hega-9) used in the crystallization setups were found at the interface between symmetry-related dimers. The presence of detergent is probably the reason that the crystal packing switched from the 12 molecules/asymmetric unit found in the IBMX complex to the four molecules found in the MERCK1 complex.

Metal Binding Sites. The metal binding sites are in a deep pocket at the interface of the three subdomains (Figures 1B and 3A); the two metals observed in this area were modeled as magnesium ions. The first metal site (MG1) appears to be fully occupied in all copies of the molecule in both complexes. It is coordinated by the side chain nitrogens of His741 (H6) and His821 (from the loop connecting H6 and H7) and the side chain oxygens of Asp822 and Asp937 (from H13; Figure 3A). The remaining two positions of the octahedral coordination are occupied by two solvent atoms, one of which also acts as a bridging ligand to the second metal ion. The occupancy of the second metal site appears to be somewhat reduced, based on the relatively higher temperature factors of the second metal, and varies among the different molecules in the asymmetric unit in both complexes. MG2 makes only one direct interaction with protein atoms, through the second side chain oxygen of

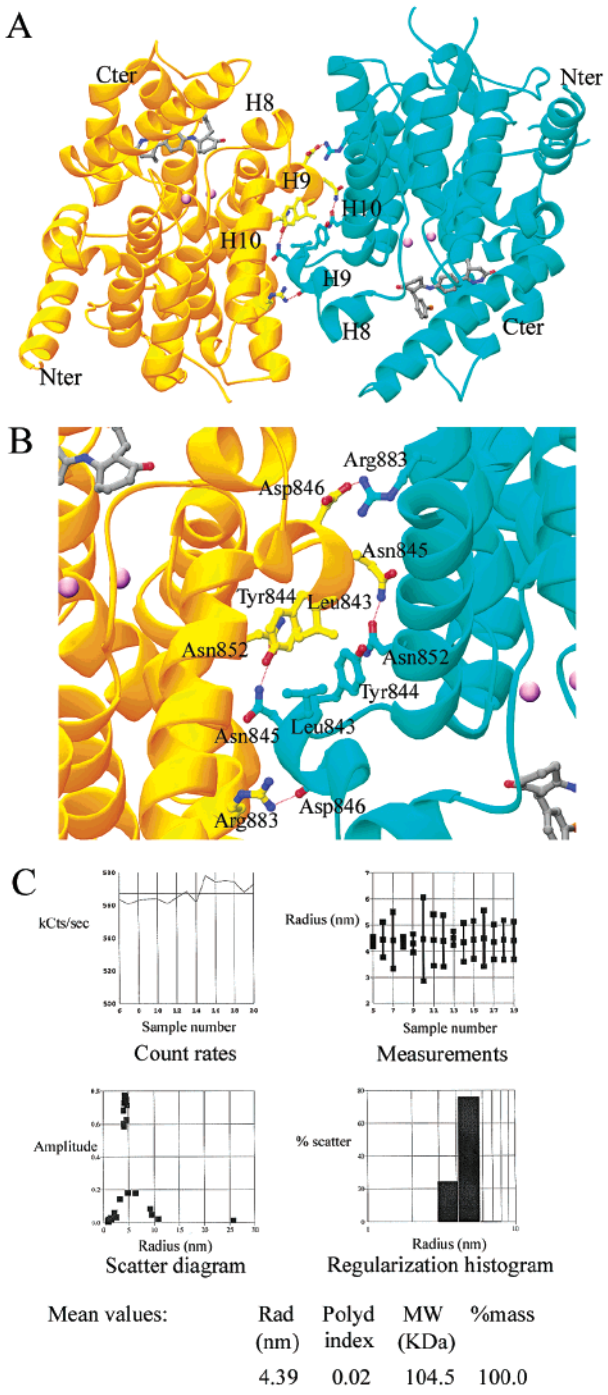

FIGURE 2: PDE3B dimer. (A) The noncrystallographic dimer found in the asymmetric unit of both PDE3B:IBMX and PDE3B:MERCK1 complexes. The helices involved in dimer formation are labeled. (B) Blow up of the dimerization interface. The residues involved in the formation of the hydrophobic core and the hydrogen bonding interactions are indicated. (C) Typical dynamic light scattering results obtained from analysis of the PDE3B samples used for crystallization. The data were analyzed and plotted using the Protein Solutions LTD Dynamics V. 4.0 software. The two upper panels report the number of counts and the estimated particle radius vs. sample number; the lower panels report the amplitude and % of scatters distribution vs. the particle radius. The mean values for the sample, as calculated by the software, are also reported. A polydispersion index ("polyd index") less than 0.10 indicates that the sample is monodisperse. The average particle radius, assuming a globular system, is 4.39 nm, corresponding to a molecular mass of about 104.5 kDa. The monomer molecular mass is approximately 42.3 kDa; this indicates that the prevalent form present in solution is most likely a dimer.

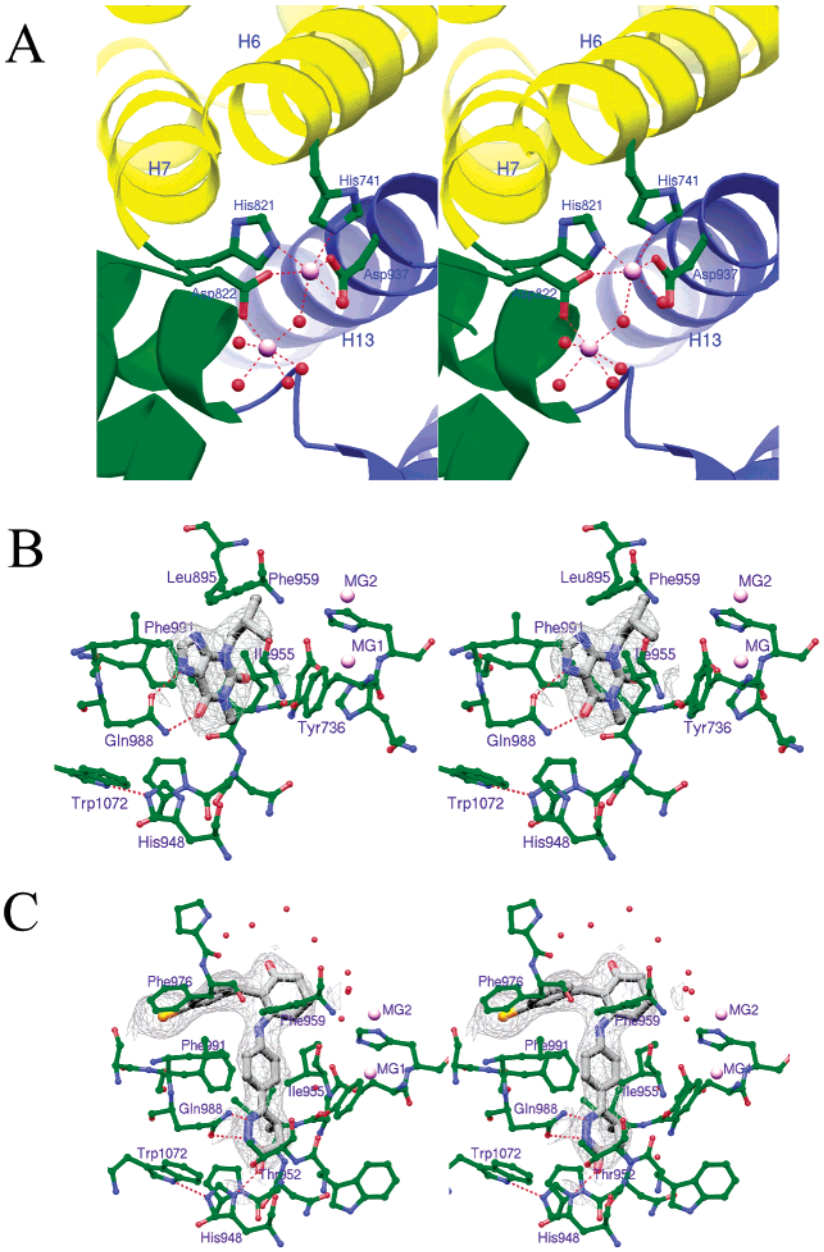

FIGURE 3: Binding of metals and inhibitors to PDE3B. Stereoview of (A) the metal binding site; (B) IBMX bound to PDE3B; and (C) MERK1 bound to PDE3B. All residues important for substrate binding and/or specificity are labeled.

Asp822. Five additional water molecules, including the bridging water, complete the MG2 octahedral coordination. These water molecules form hydrogen bond interactions with the side chains of Asp822, Glu851, His737, His825, and Thr893, and the main chain oxygens of His821 and Thr893.

Inhibitor Binding Site. The inhibitor binding site in both complexes is located in the cradle formed by helices H14 and H15 and is completely nonoverlapping with the metal binding sites (Figures 1B and 3B,C). IBMX is a purine-derived, competitive inhibitor of most known PDEs, although it is ineffective for inhibition of PDE8 and PDE9 (*2*). IBMX makes two hydrogen bond interactions with the side chain of the highly conserved Gln988. The xanthine ring is stacked against the side chains of Phe991 and Ile955. The side chain of Tyr736 also contributes to the formation of the hydrophobic pocket containing the xanthine ring. The isobutyl chain lies in a wide pocket formed by the side chains of Tyr736, His737, Leu895, and Phe959. At the far end of this pocket (about 6.3 Å away from the bound inhibitor) is the metal binding site. The MERCK1 inhibitor is bound in an extended conformation, with the central aromatic ring overlapping the xanthine ring of IBMX. The dihydropiridazinone moiety sits in a very tight pocket formed by the main chain atoms of residues Ile938-Pro941 (from H13) and Lys950-Thr952 (from H14) and the side chain of His948. The dihydropiridazinone nitrogens form hydrogen bonds to the side chain of Gln988 similar to those seen in the IBMX complex, but the side chain of Gln988 assumes the opposite conformation, similar to that observed in the PDE4 structures (*12*, *13*). The exocyclic oxygen interacts with the side chains of Thr952 and His948, which is held in the correct orientation by a hydrogen bond with the side chain nitrogen of Trp1072. The exocyclic methyl binds in a hydrophobic pocket formed by residues Ile938-Pro941. The benzyl ring is stacked between the side chains of Phe991 and Ile955. The 1,3-hexadione sits approximately in the same area as the isobutyl

chain of IBMX, about 6.4 Å from the metal ions. The 2-aryl substituent extends into a nearby hydrophobic pocket formed by the side chains of Phe959, Pro975, Phe976, Met977, Leu987, Ser990, and Phe991. One end of this pocket is exposed to solvent in the current structure, and several ordered water molecules are bound there.

DISCUSSION

Comparison with the PDE4 and PDE5 Structures. Our model of the enzyme monomer contains residues 659−766, 782−1015, and 1053−1073, arranged in a compact structure containing 16 α-helices, numbered H1−H16 in Figure 1B. This tertiary structure is very similar to the one described for the original PDE4B structure (*11*) and the subsequent PDE4D (*12*, *13*) and PDE5A (*14*) structures, although PDE3B has only limited sequence identity with PDE4 and PDE5 in the catalytic domain (25.2 and 17.8%, respectively). The coordinates for the PDE5 structure are not available at this time, and the PDE4B and PDE4D structures are highly similar; hence, the following comparison is made with PDE4B. The two structures align with an RMSD of 0.718 Å for 288 CA atoms [calculated with LSQMAN (*22*)], and the similarity between the two enzymes is sufficiently strong that we successfully used a core PDE4 structure as a model for the molecular replacement procedure used to solve the PDE3B structure. The architecture of the substrate and metal binding sites is basically identical in the two enzymes, although there are differences in protein sequence that correlate with the substrate and inhibitor specificity (see below). The major differences in tertiary structure are localized at the opposite end of the molecules and involve mainly the position of helix H1 and the loops connecting helices H12 and H13. In both PDE3 isoforms, there are also two long inserts (the PDE3 specific 44 residue insert between H6 and H7 and a 52 residue insert between H15 and H16) that have no counterpart in PDE4. PDE4 H17 overlaps with the inhibitor binding site and has no equivalent in the PDE3 structure, although we cannot rule out that part of the missing, presumably disordered, loops may occupy a similar position.

In both PDE3B complexes, the same noncrystallographic dimer has been identified in the asymmetric unit (Figure 2A,B). A dimeric species was evident in dynamic light scattering experiments carried out at the concentration used for crystallization (Figure 2C), and it has been reported that all mammalian PDEs appear to exist as dimers of two catalytic subunits (*1*). Both the N- and the C-termini of the catalytic domain are localized on the opposite side with respect to the dimerization domain (Figure 2A), suggesting that the dimer observed here could also be formed in the full length enzyme. The identical dimeric arrangement and a very similar hydrogen bonding network have also been observed in the structure of PDE4D (*12*, *13*). The dimer interface is the most conserved surface aside from the active site pocket, and mutations of residues located at the dimer interface have been shown to disrupt oligomerization in solution (*12*), suggesting that dimerization is not a crystallization-induced artifact. Although it is not possible to state with absolute certainty that the dimer observed in the structures is the physiological dimer formed by the full length enzyme, the available structural and mutagenesis data strongly suggest that it could be.

Metal Binding Sites in PDE3B. Seven of the PDE subfamilies require divalent metal cations for catalytic activity (*23*). In both PDE4 and PDE5, a zinc ion has been identified as the metal present in the primary metal binding site, and this assignment is consistent with the fact that zinc is required for catalysis for both enzymes (*24*). The PDE3A activity is dependent on the presence of $Mn^{2+} > Mg^{2+} > Co^{2+}$; in contrast with PDE4 and PDE5, Zn^{2+} has been shown to have an inhibitory effect on the enzyme (*23*). Similarly, with the PDE3B isoform, we observed that a combination of Mg^{2+} and Mn^{2+} was required for optimal catalysis (data not shown). On the basis of the relative temperature factors and on the fact that the protein was refolded in the presence of 20 mM $MgCl_2$ (*9*) and crystallized in the presence of 200 mM $MgSO_4$ (*15*), the two metals were refined as magnesium ions. Although the available data do not unambiguously establish the exact nature of the metal ions bound to PDE3B and it does appear that there could be some flexibility in metal binding, the refinement statistics clearly indicate that magnesium is present in both binding sites and that zinc is not present in our models. All PDEs contain a PDE specific sequence motif, $^{821}HD(X)_2H(X)_4N^{830}$ (human PDE3B numbering) and two consensus metal binding domains [$H(X)_3H(X)_{24-26}E$], one of which partially overlaps with the PDE motif (*1*, *25*). In PDE3B, as in PDE4 and PDE5, the metal binding site is formed by residues belonging to both consensus sequences. His741 belongs to the first motif, $^{737}H(X)_3H(X)_{69}E^{810}$, and the number of residues separating the second histidine residue from the glutamic acid residue in PDE3 is larger than the 24−26 normally observed in other PDEs because of the PDE3 specific 44 residue insert between helices H6 and H7. Two other metal ligands, His821 and Asp822, are the first and second residue in the PDE specific sequence motif. The fourth ligand, Asp937, is 115 residues downstream from His821 and has not previously been implicated in metal binding, although its importance in inhibitor binding and enzyme catalysis in PDE3A had been established by mutagenesis studies (*26*). The structural results indicate that the residue may play a similar role in PDE3B.

Structural Basis for Substrate Specificity. Several PDE families are highly selective for either cAMP (PDE4, PDE7, and PDE8) or cGMP (PDE5, PDE6, and PDE9), while PDE3, together with PDE1, PDE2, PDE10, and PDE11, accommodates both. The hydrogen bonding character at the 1- and 6-positions in cAMP and cGMP is reversed (Figure 4, top panel). The specificity of PDE4 for cAMP and PDE5 for cGMP has been related to the ability of the side chain of the completely conserved glutamine residue to accept and donate hydrogen bonds and to the hydrogen bonding interactions with nearby residues that hold that side chain in the correct configuration (*11*, *14*). In the recently reported structure of AMP bound to PDE4D, the adenine N1 (a hydrogen bond acceptor) is hydrogen-bonded to the side chain nitrogen of Gln369 (corresponding to Gln443 in PDE4B), a hydrogen bond donor. This side chain is held in this configuration by an interaction with Tyr329 (Tyr403 in PDE4B). Position N1 in cGMP is also a hydrogen bond donor, and binding of this nucleotide in a manner similar to that observed for cAMP is highly unlikely. Conversely, in PDE5, the residue corresponding to Tyr403 and Tyr329 is Gln775, and this residue holds Gln817 in the opposite orientation, so that the hydrogen bonding character is

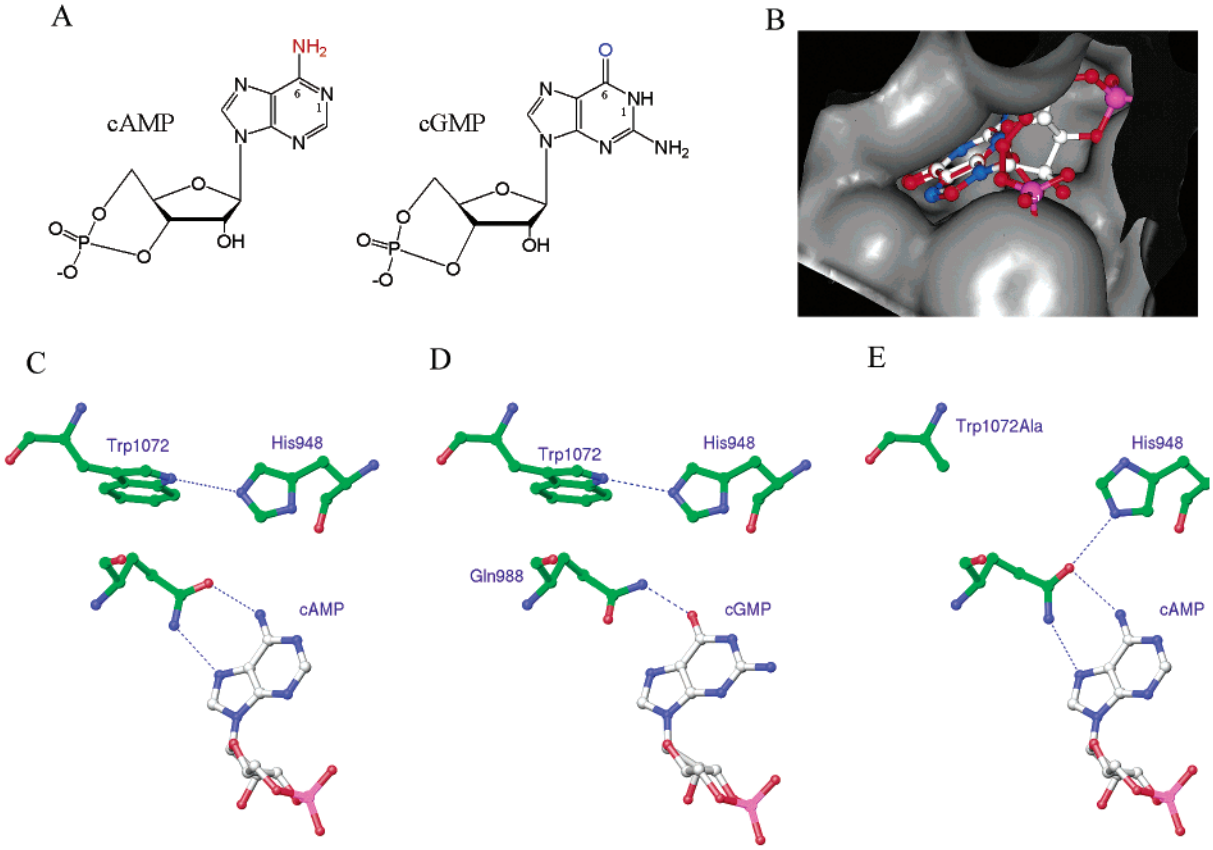

FIGURE 4: PDE3B dual nucleotide specificity. (A) The chemical structures of cAMP and cGMP: the hydrogen bonding donor−acceptor character at positions 1 and 6 is reversed in the two nucleotides. (B) Surface representation of the PDE3B binding site. cGMP in syn (white) and anti (red) conformation is displayed as a ball-and-stick model. The syn conformation is complementary to the shape of the binding site, while the anti conformation shows steric clashes with the sides of the binding site. (C,D) In PDE3B, the side chain of His948 is held by a hydrogen bond to Trp1072; consequently, the side chain of Gln988 is free to rotate and can assume a configuration that is compatible with both cAMP and cGMP. (E) In the Trp1072Ala mutant, the side chain of His948 is released and can interact with Gln988, through its side chain oxygen. Gln988 is now held in a configuration that would allow binding of cAMP but would greatly disfavor cGMP binding.

complementary to cGMP (*14*). In PDE3, the conserved Gln988 does not interact with any nearby residue, and it is free to assume both conformations (as observed in the two structures reported here, Figure 3B,C). The residue corresponding to PDE4 Tyr403 and PDE5 Gln775 is His948 in PDE3, and this side chain is ~3.4 Å from the side chain of Gln988. Although it is conceivable that a different side chain conformation could allow His948 to interact with and influence the conformation of Gln988, we observe it to be in only one conformation, stabilized by a hydrogen bond with the side chain of Trp1072 and not interacting with Gln988. We modeled both cAMP and cGMP in the PDE3B binding site, based on the similarity of the purine ring of the nucleotides to the hypoxanthine ring of IBMX, the mutagenesis data (*27*, *28*), and the shape of the binding site (Figure 4B): the best fitting was achieved with the two nucleotides in a syn conformation and interacting with the side chain of Gln988 through the 6-position (Figure 4C,D). In the PDE4D:AMP complex, the AMP adenine interacts with Gln369 through N1: the different orientation of the adenine ring is likely due to the presence of a second interaction with the side chain of Asn321; in PDE3B, the corresponding residue is Gly940, and the lack of a polar side chain in this position is clearly going to affect the nucleotide binding mode. The orientation of the side chain of Gln988 in the AMP complex was assumed to be the one observed in the cAMP specific PDE4, but because it is free to rotate, it can complement either nucleotide, thus explaining the lack of nucleotide selectivity displayed by the enzyme. In addition, a second hydrogen bond is possible from the side chain nitrogen of Gln988 to position 7 of cAMP.

Effects of Mutagenesis on Activity and Substrate Binding. Several mutagenesis experiments have attempted to address substrate and inhibitor specificity in the PDE3 family. Although most of these studies were done using PDE3A, the two isoforms are so similar in the catalytic domain that the conclusions can be likely applied to both enzymes. Work done in the past few years identified several residues apparently involved in catalysis and/or binding of substrate and inhibitors, summarized in Table 2 and visualized in Figure 5. Most of the mutations appear to affect in some way the catalytic activity of the enzyme, while different residues seem to have different effects on binding of cAMP and cGMP. The effect of the mutations on inhibitor binding will be discussed below. Residues that affect the catalytic activity are colored green in Figure 5, and the crystal structure reveals that they all are involved, either directly (as His741, His821, and Asp937) or through primary or secondary hydrogen bonding interactions (as His737, His825, Glu851, and Glu958) in the formation and stabilization of the metal binding sites. Mutation of Tyr736 also results in a decrease in activity: this residue is positioned directly above the side chain of His737, where it presumably helps maintain the hydrogen bonding pattern. The effect on catalytic activity

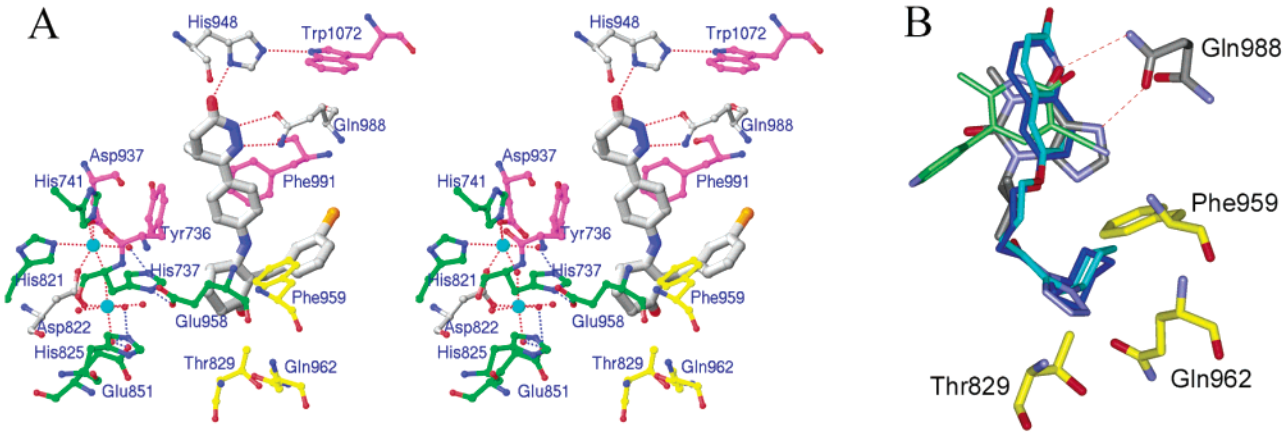

FIGURE 5: Mutagenesis analysis of residues surrounding the metal and inhibitor binding site in PDE3B. (A) The residues comprising the metal and inhibitor binding site in PDE3B. Residues important in binding but not previously identified by mutagenesis analysis are in gray, as is the inhibitor MERCK1. Residues identified by mutagenesis analysis are color coded. Green: residues that affect the catalytic activity of the enzyme. Magenta: residues that affect binding of all inhibitors tested. Yellow: residues that affect binding of cilostamide and cilostazol only. (B) The inhibitors milrinone (green), cilostamide (blue), and cilostazol (cyan) have been modeled in the PDE3B binding site based on IBMX (gray) binding. Only cilostamide and cilostazol extend toward Thr829, Phe959, and Gln962.

Table 2: Mutagenesis Analysis of Residues that Are Part of the cAMP/cGMP Binding Site or Involved in Catalysis in the PDE3 Family[a]

residue (PDE3B)	residue (PDE3A)	K_{cat}	cAMP binding	cGMP binding	inhibitor binding	ref
Tyr736	Tyr751	↓	no effect	↓	M ↓ CE ↓	(*27*, *28*)
His737	His752	↓	no effect	no effect	M: no effect	(*26*)
His741	His756	↓	no effect	no effect	M: no effect	(*26*)
Glu810	Glu825	↓	no effect	no effect	M: no effect	(*26*)
His821	His836	↓	no effect	↓	M: no effect	(*27*, *28*)
His825	His840	↓	no effect	↓	ND	(*25*, *27*)
Thr829	Thr844	no effect	no effect	no effect	M: no effect CL ↓	(*28*)
Glu851	Glu866	↓	↓	↓	M: no effect	(*26*)
Asp937	Asp950	↓	no effect	↓	M ↓ CL ↓	(*27*, *28*)
Glu958	Glu971	↓	no effect	no effect	M: no effect	(*26*)
Phe959	Phe972	↓	no effect	no effect	M: no effect CL: ↓	(*28*)
Gln962	Gln975	↓	no effect	no effect	M: no effect CL ↓	(*28*)
Phe991	Phe1004	↓	↓	↓	M ↓ CL ↓	(*27*, *28*)
Trp1072	Trp1086	no effect	↓	↓	M ↓ CE ↓	(*10*)

[a] The mutations are all to alanine residues except for Trp1072, which was mutated to both tyrosine and alanine. Inhibitors used in binding assays are milrinone (M), cilostamide (CE), or cilostazol (CL). ND: not determined.

caused by mutations at residues Glu810, Phe959, and Gln962 is difficult to explain based on the current structure, since most of these residues are far from the metal and substrate binding sites, but it is possible that small differences between the structures of the two isoforms may account for such results. cAMP binding is affected only by mutations at Glu851, Phe991, and Trp1072; for Phe991 and Trp1072, these results are consistent with the roles that these residues have been shown to play in the crystal structure. Phe991 forms part of the hydrophobic pocket occupied by the aromatic rings of inhibitors and presumably by the purine ring of the nucleotides. Trp1072 indirectly influences the position of the side chain of Gln988; the fact that the Trp1072Tyr mutation only decreases the K_m for cAMP by about 2-fold and the Trp1072Ala decreases it by about 6-fold suggests that a large hydrophobic side chain at position 1072 is probably required in order to limit the Gln988 side chain motion. The role of Glu851 in substrate binding is not completely clear from the inhibitor-bound crystal structure. cGMP binding appears to be more affected by mutagenesis than cAMP binding. The effect of the mutation of Tyr736 (Table 2) can be explained considering that cGMP has an exocyclic amine in position 2, which is absent in cAMP. In our model of cGMP bound to PDE3B, the amine has been positioned within hydrogen bonding distance of the side chain of Tyr736. Mutation of this residue to alanine would remove the hydrogen bond potentiality and thus reduce cGMP binding. The presence of this additional interaction may also constrain cGMP in a position that would require an intact metal binding site for productive binding. This could explain the loss of cGMP binding observed upon mutations of residues His821, His825, Glu851, and Asp937. The effect of Trp1072 mutations on cGMP is consistent with the requirement for a hydrogen bond between Trp1072 and His948. In the absence of this hydrogen bond, the side chain of His948 could be able to interact with the side chain of Gln988. Because of the hydrogen bond directionality, the side chain of Gln988 would then be held in an orientation that would permit interaction with cAMP but inhibit binding of cGMP, thus explaining the 12- and 740-fold reduction on IC_{50} for the Trp1072Tyr and Trp1072Ala mutations [Figure 4 C−E (*10*)]. The fact that the Trp1072Tyr mutation affects the IC_{50} to a lesser extent than the Trp1072Ala mutation suggests that the tyrosine may still be able to hydrogen bond to His948, thus allowing to some extent cGMP binding.

Inhibitor Binding and Specificity. Many known PDE3 inhibitors have a pyridazinone core that has been shown to be important for selectivity over other PDEs [e.g., PDE2, PDE4, and PDE7 (*29*)]. Two PDE3 specific inhibitors that have been tested against PDE3B are milrinone and cilostamide (Figure 1A). Dihydropyridazinones and dimethylpyrazolones have been reported to be more potent than milrinone, and recently, Edmondson et al. (*29*) reported two series of potent and selective PDE3B inhibitors derived from this class. MERCK1 is one such compound, with an IC_{50} of 0.27 nM for the refolded 654−1073 fragment of PDE3B and of

Table 3: Inhibition of PDE3B (387−1112) and PDE3A (388−1112) by Dihydropyridazinones (*29*)

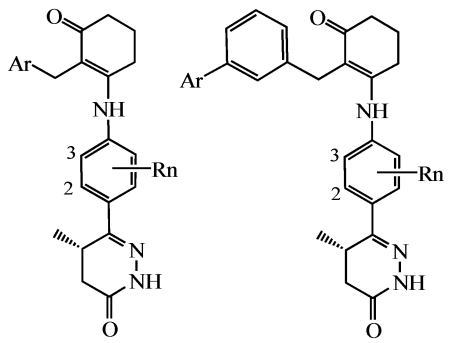

1

2

entry	Ar	Rn	PDE3B IC_{50} (nM)	PDE3A IC_{50} (nM)
1a	H	H	8.8	44
1b	Ph	H	0.19	1.3
1c (MERCK1)	3-IPh	H	0.11	0.33
1d	2-MeOPh	H	0.13	0.39
2a	3-thiophene	H	0.068	0.11
2b	3-NO_2Ph	H	0.049	0.11
1e	Ph	2-Me	2.6	22
1f	Ph	2-Et	21	101
1g	Ph	2-Cl	4.8	46
1h	Ph	3-Me	0.61	3.7
1i	Ph	2-F	0.24	1.6
1j	Ph	3-F	0.26	1.2
1k	Ph	2,5-F2	0.62	1.6

0.11 nM for the 387−1112 solubly expressed enzyme. The structure−activity relationship (Table 3) (*29*) displayed by this class of compound can be explained by the several hydrogen bonding and hydrophobic interactions made by MERCK1 with PDE3B. For example, it was noted that large hydrophobic groups in place of the iodine substantially increase the potency of the compounds (Table 3, compounds **2a**,**b**); this observation is consistent with the fact that the 2-aryl substituent extends into a large hydrophobic pocket and that increasing the size of the group would optimize interactions with the protein. Similarly, it was noted that large substitutions at position 2 in the central phenyl ring (compounds **1e**−**g**) decrease potency, and this finding is consistent with the fact that this position is located in a constricted area of the binding site. Conversely, the presence of smaller substituents such as fluorine atoms on the ring may optimize the interactions with the hydrophobic pocket and maintain sub-nanomolar affinity (compounds **1i**−**k**). The high selectivity of dihydropyridazinones for PDE3 over other PDEs [e.g., PDE4, PDE5, and PDE7 (*29*)] can be attributed to the hydrogen bond interaction made by the pyridazinone carbonyl oxygen and the side chain of His948. PDE4 and PDE5 have a tyrosyl or a glutaminyl residue in the corresponding position. In both cases, these residues are involved, through a network of hydrogen bonds, in positioning the side chain of the conserved glutamine (Gln988 in PDE3) so that it can recognize cAMP or cGMP, respectively (*11*, *14*). In addition to the fact that these two residues would be too large to accommodate the inhibitor, they also would not be able to interact with the ligand. The histidine side chain, specific to PDE3, provides both the room and the hydrogen bonding pattern necessary for specific inhibitor binding. The side chain of His948 is maintained in the correct orientation by a unique hydrogen bond interaction with the side chain of Trp1072. Mutation of Trp1072 to tyrosine reduces the affinity of MERCK1 of about 2-fold, while the corresponding Trp1072Ala mutant reduces it of about 90-fold (Tota, M., and Chung, C. Personal communication). This is again consistent with the fact that a hydrogen bond interaction between the residue at position 1072 and His948 is required, in this case to position the side chain of His948 in the right orientation to hydrogen bond to the carbonyl oxygen of the inhibitor, rather than influence the orientation of Gln988. The Trp1072Tyr and Trp1072Ala mutations have also been shown to affect binding of other inhibitors, such as IBMX, milrinone, and cilostamide (*10*). Modeling of cilostamide, cilostazol, and milrinone indicates that all three inhibitors bind as IBMX, i.e., with the carbonyl oxygen hydrogen-bonded to Gln988. Because the hydrogen bond directionality of the inhibitors resembles that of cGMP, the effect of the mutation can be explained by the same mechanism, i.e., the release of the side chain of His948, which is now capable of interacting with Gln988 and holding it in a configuration that will not allow binding of cGMP or the inhibitors. IBMX is an interesting exception, because the Trp1072Ala mutation does not affect its binding as much as it would be expected (*10*), based on the fact that the Gln988 side chain orientation in the IBMX complex is identical to that postulated for cGMP binding. One possible explanation of this phenomenon could be a different binding orientation for IBMX to the mutant enzyme, i.e., in the orientation that would be complementary to the flipped side chain of Gln988. The idea that multiple binding modes may be allowed for IBMX is supported by the fact that this compound is an inhibitor for both cAMP and cGMP specific PDEs (*2*). In addition, docking of IBMX to either the PDE3B binding site observed in the crystal structure or to a PDE3B binding site, in which the side chain of Gln988 was modeled as in a "cAMP" complex, indicates that the two IBMX orientations maintain similar binding interactions (data not shown).

Binding of all inhibitors tested is also decreased by mutation at Tyr736, Asp937, and Phe991 (in magenta in Figure 5; Table 2). These residues are part of the hydrophobic pocket where the IBMX xanthine ring and the central aromatic ring of MERCK1 are located and thus are a substantial part of the binding site. In addition, our modeling shows that for milrinone the pyridine ring extends toward the metal binding site, within hydrogen bonding distance of Asp937. Mutation of residues Thr829, Phe959, and Gln962 (in yellow in Figure 5; Table 2) affects only binding of larger inhibitors, such as cilostamide and cilostazol, but has no effect on binding of cGMP or the smaller inhibitor milrinone. These three residues are located near the solvent-exposed area where the 2-aryl substituent of MERCK1 is located. In our (Figure 5B) model and similar models (*28*), the cyclehexyl amido and the cycle-hexyl-tetrazole of cilostamide and cilostazol extend toward Thr829, Phe959, and Gln96; it is then reasonable to assume that mutation of these residues could affect binding of these ligands, consistently with the mutagenesis results.

Conclusions. The structures reported here provide a structural explanation for the PDE3 family's unusual dual nucleotide affinity, as well as the specificity of certain inhibitors for PDE3 over members of other PDE families. Although the reported inhibitors show a consistent 3−8-fold

subtype specificity, the structural reasons for this are not immediately obvious from the available structures. Subtype selectivity may be related to the postioning of the two inserts that are disordered in the current structure: these regions represent the areas where the major sequence differences between the A and the B isoform catalytic domains are located. It is also possible that in the full length enzyme, other regions of the polypeptide chain interact with the binding site, thus contributing to the specificity. Modifications on the inhibitors that seem to consistently increase the subtype specificity (such as those on the central aromatic ring, compounds **1e**−**k** in Table 3) may cause small rearrangement of the inhibitor itself in the binding area, with a consequent change in the position of the substituted vinylogous amide. This area of the binding site is occupied by helix H17 in the PDE4 structure; it is conceivable that in PDE3 it could be covered by portions of the noncatalytic domain, which could provide more specific interactions with the inhibitor.

ACKNOWLEDGMENT

We thank the staff at the facilities at the Industrial Macromolecular Crystallography Association Collaborative Access Team (IMCA-CAT) for help during data collection.

NOTE ADDED IN PROOF

While this paper was in press, two more papers reporting structures of PDE4 and PDE5 have been published (ref *31*, confirming that multiple binding modes for IBMX are indeed possible, and ref *32*).

REFERENCES

1. Beavo, J. A. (1995) Cyclic Nucleotide phosphodiesterases: functional implications of multiple isoforms, *Physiol. Rev. 75*, 725−743.
2. Francis, S. H., Turko, I. V., and Corbin, J. D. (2001) Cyclic nucleotide phosphodiesterases: relating structure and function, *Prog. Nucleic Acid Res. Mol. Biol. 65*, 1−52.
3. Reinhardt, R. R., Chin, E., Zhou, J., Taira, M., Murata, T., Manganiello, V. C., and Bondy, C. A. (1995) Distinctive anatomical patterns of gene expression for cGMP-inhibited cyclic nucleotide phosphodiesterases, *J. Clin. Invest. 95*, 1528−1538.
4. Harndahl, L., Jing, X.-J., Iversson, R., Degerman, E., Ahren, B., Manganiello, V. C., Renstrom, E., and Stenson Holst, L. (2002) Important role of phosphodiesterase 3B for the stimulatory action of cAMP on pancreatic beta-cell exocytosis and release of insulin, *J. Biol. Chem. 277*, 37446−37455.
5. Elks, M. L., and Manganiello, V. C. (1984) Selective effects of phosphodiesterase inhibitors on different phosphodiesterases, adenosine 3′,5′-monophosphate metabolism, and lipolysis in 3T3-L1 adipocytes, *Endocrinology 115*, 1262−1268.
6. Synder, P. B. (1999) The adipocyte cGMP-inhibited cyclic nucleotide phosphodiesterase (PDE3B) as a target for lipolytic and thermogenic agents for the treatment of obesity, *Emerging Ther. Targets 3*, 587−599.
7. He, R., Komas, N., Ekholm, D., Murata, T., Taira, M., Hockman, S., Dergerman, E., and Manganiello, V. C. (1998) Expression and characterization of deletion recombinants of two cGMP-inhibited cyclic nucleotide phosphodiesterases (PDE-3), *Cell Biochem. Biophys. 29*, 89−111.
8. Shakur, Y., Takeda, K., Kenan, Y., Yu, Z. X., Rena, G., Brandt, D., Houslay, M. D., Degerman, E., Ferrans, V. J., and Manganiello, V. C. (2000) Membrane localization of cyclic nucleotide phosphodiesterase 3 (PDE3). Two N-terminal domains are required for the efficient targeting to, and association of, PDE3 with endoplasmic reticulum, *J. Biol. Chem. 275*, 38749−38761.
9. Varnerin, J. P., Chung, C. C, Patel, S. B., Scapin, G., Parmee, E. R., Morin, N., MacNeil, D., Cully, D. F., Van der Ploeg, L., and Tota, M. R. (2004) Expression, refolding and purification of recombinant human phosphodiesterase 3B: definition of the N-terminus of the catalytic core, *Protein Expression Purif.* In press.
10. Chung, C., Varnerin, J., Morin, N. R., MacNeil, D. J., Singh, S. B., Patel, S., Scapin, G., Van der Ploeg, L., and Tota, M. R. (2003) The role of tryptophan 1072 in PDE3B inhibitor binding, *Biochem. Biophys. Res. Commun. 307*, 1045−1050.
11. Xu, R. X., Hassell, A. M., Vanderwall, D., Lambert, M. H., Holmes, W. D., Luther, M. A., Rocque, W. J., Milburn, M. V., Zhao, Y., Ke, H., and Nolte, R. T. (2000) Atomic structure of PDE4: insights into phosphodiesterase mechanism and specificity, *Science 288*, 1822−1825.
12. Lee, M. E., Markowitz, J., Lee, J. O., and Lee, H. (2002) Crystal structure of phosphodiesterase 4D and inhibitor complex, *FEBS Lett. 530*, 53−58.
13. Huai, Q., Colicelli, J., and Ke, H. (2003) The crystal structure of AMP-bound PDE4 suggests a mechanism for phosphodiesterase catalysis, *Biochemistry 42*, 13220−13226.
14. Sung, B.-J., Hwang, K. Y., Jeon, Y. H., Lee, J. I., Heo, Y.-S., Kim, J. H., Moon, J., Yoon, J. M., Hyun, Y.-L., Kim, E., Eum, S. J., Park, S.-Y., Lee, J.-O., Lee, T. G., Ro, S., and Cho, J. M. (2003) Structure of the catalytic domain of human phosphodiesterase 5 with bond drug molecules, *Nature 425*, 98−101.
15. Patel, S. B., Varnerin, J. P., Tota, M. R., Edmondson, S. D., Parmee, E. R., Becker, J. W., and Scapin, G. (2003) Crystallization and preliminary X-ray diffraction analysis of the catalytic domain of recombinant human phosphodiesterase 3B, *Acta Crystallogr. D60*, 169−171.
16. Otwinowski, Z., and Minor, W. (1997) Processing of X-ray diffraction data collected in oscillation mode, *Methods Enzymol. 276*, 307−326.
17. Vagin, A., and Teplyakov, A. (1997) MOLREP: an automated program for molecular replacement, *J. Appl. Crystallogr. 30*, 1022−1025.
18. Collaborative Computational Project, N. (1994) The CCP4 suite: programs for protein crystallography, *Acta Crystallogr. D50*, 760−763.
19. Jones, A. T., and Kjeldgaard, M. (1997) Electron density map interpretation, *Methods Enzymol. 277*, 173−208.
20. Brünger, A. T., Adams, P. D., Clore, G. M., DeLano, W. L., Gros, P., Grosse-Kunstleve, R. W., Jiang, J.-S., Kuszewski, J., Nilges, M., Pannu, N. S., Read, R. J., Rice, L. M., Simonson, T., and Warren, G. L. (1998) Crystallography & NMR system: a new software suite for macromolecular structure determination, *Acta Crystallogr. D54*, 905−921.
21. Degerman, E., Belfrage, P., and Manganiello, V. C. (1997) Structure, localization, and regulation of cGMP-inhibited phosphodiesterase (PDE3), *J. Biol. Chem. 272*, 6823−6826.
22. Kleywegt, G. J., Zou, J. Y., Kjeldgaard, M., and Jones, T. A. (2001) in *International Tables for Crystallography. Crystallography of Biological Macromolecules* (Rossmann, M. G. a. A. E., Ed.) pp 353−356, 366−367, Kluwer Academic Publishers, Dordrecht, The Netherlands.
23. Omburo, G. A., Brickus, T., Ghazaleh, F. A., and Colman, R. W. (1995) Divalent metal cation requirement and possible classification of cGMP-inhibited phosphodiesterase as a metallohydrolase, *Arch. Biochem. Biophys. 323*, 105.
24. Francis, S. H., Colbran, J. L., McAllister-Lucas, L. M., and Corbin, J. D. (1994) Zinc interactions and conserved motifs of the cGMP-binding cGMP specific phosphodiesterase suggest that it is a zinc hydrolase, *J. Biol. Chem. 269*, 22477−22480.
25. Cheung, P. P., Yu, L., Zhang, H., and Colman, R. W. (1998) Partial characterization of the active site human platelet cAMP phosphodiesterase, PDE3A, by site-directed mutagenesis, *Arch. Biochem. Biophys. 360*, 99−104.
26. Zhang, W., and Colman, R. W. (2000) Conserved amino acids in metal-binding motifs of PDE3A are involved in substrate and inhibitor binding, *Blood 95*, 3380−3386.
27. Zhang, W., Ke, H. M., Tretiakova, A. P., Jameson, B., and Colman, R. W. (2001) Identification of overlapping but distinct cAMP and cGMP interaction sites with cyclic nucleotide phosphodiesterase 3A by site-directed mutagenesis and molecular modeling based on crystalline PDE4B, *Protein Sci. 10*, 1481−1489.
28. Zhang, W., Ke, H., and Colman, R. W. (2002) Identification of interaction sites of cyclic nucleotide phosphodiesterase type 3A with milrinone and cilostazol using molecular modeling and site-directed mutagenesis, *Mol. Pharmacol. 62*, 514−520.
29. Edmondson, S. D., Mastracchio, A., He, J., Chung, C. C., Forrest, M. J., Hofsess, S., Macyntire, E., Metzger, J., O'Connor, N., Patel, K., Tong, X., Tota, M. R., Van Der Ploeg, L. H. T., Varnerin, J.

P., Fisher, M. H., Wyvratt, M. J., Weber, A. E., and Parmee, E. R. (2003) Benzyl vinylogous amide substituted aryldihydropyridazinones and aryldimethylpyrazolones as potent and selective PDE3B inhibitors, *Bioorg. Med. Chem. Lett. 13*, 3983−3987.
30. Carson, M. (1997) Ribbons, *Methods Enzymol. 277*, 493−505.
31. Huai, Q., Liu, Y., Francis, S. H., Corbin, J. D., and Ke, H. (2004) Crystal Structures of Phosphodiesterases 4 and 5 in Complex with Inhibitor 3-Isobutyl-1-methylxanthine Suggest a Conformation Determinant of Inhibitor Selectivity. *J. Biol. Chem. 279*, 13095−13101.
32. Xu, R. X., Rocque, W. J., Lambert, M. H., Vanderwall, D. E., Luther, M. A., and Nolte, R. T. (2004) Crystal Structures of the Catalytic Domain of Phosphodiesterase 4B Complexed with AMP, 8-Br-AMP, and Rolipram. *J. Mol. Biol. 337*, 355−365.

BI049868I